

Published in final edited form as:

Ultrasound Med Biol. 2011 June ; 37(6): 980–995. doi:10.1016/j.ultrasmedbio.2011.03.004.

Imaging of Wall Motion Coupled with Blood Flow Velocity in the Hearts and Vessels *in vivo*: A Feasibility Study

Jianwen Luo* and Elisa E. Konofagou*[†]

* Department of Biomedical Engineering, Columbia University, New York, NY

[†] Department of Radiology, Columbia University, New York, NY

Abstract

The mechanical property and geometry changes as a result of disease affect both the wall motion and blood flow, while the latter two are also coupled and therefore continuously influence one another. Simultaneous and registered imaging of both cardiovascular wall motion and blood velocity may thus contribute to more complete computational models of cardiovascular mechanical and fluid dynamics as well as provide additional diagnostic information. The objective of this paper is to determine the feasibility of imaging cardiovascular wall motion coupled with blood flow *in vivo*. Normal (n=6) and infarcted (n=5) murine left ventricles, and normal (n=5) and aneurysmal (n=4) murine abdominal aortas, were imaged in longitudinal views with a 30-MHz ultrasound probe. Using electrocardiogram (ECG) gating, two-dimensional (2-D) radio-frequency (RF) data were acquired at a frame rate of 8 kHz. The axial wall velocity and blood velocity were estimated using a speckle tracking technique. Spatially and temporally registered imaging of both cardiovascular wall motion and blood flow was shown feasible. Reduced wall motion was detected in the infarcted region, while vortex flow patterns were imaged in diastolic phases of both normal and infarcted left ventricles. The myocardial wall motion and blood flow were found to be more synchronized in the normal heart, where the blood moves towards the anteroseptal wall after the mitral valve opens (i.e., rapid filling phase), and the anteroseptal wall simultaneously undergoes outward motion. In the infarcted heart, however, in the rapid filling phase the basal anteroseptal wall starts moving, about 20 ms before the mitral valve opens and the blood enters the left ventricle. In the normal aorta, the wall motion and blood velocity were uniform and synchronized. In the aneurysmal aorta, reduced and spatially varied wall motion and vortex flow patterns in the aneurysmal sac were found. The wall motion and blood velocity were thus less synchronized in the aneurysmal aorta. Cardiovascular wall motion and blood flow were both imaged in mice *in vivo*. This dual information may provide important information for the diagnosis of cardiovascular disease as well as essential parameters for biomechanical modeling.

© 2011 World Federation for Ultrasound in Medicine and Biology. Published by Elsevier Inc. All rights reserved.

Corresponding Author: Elisa E. Konofagou, Ph.D. Department of Biomedical Engineering, Columbia University, 351 Engineering Terrace, mail code 8904, 1210 Amsterdam Avenue, New York, NY 10027. Phone: 212-342-0863. Fax: 212-342-5773. ek2191@columbia.edu.

Publisher's Disclaimer: This is a PDF file of an unedited manuscript that has been accepted for publication. As a service to our customers we are providing this early version of the manuscript. The manuscript will undergo copyediting, typesetting, and review of the resulting proof before it is published in its final citable form. Please note that during the production process errors may be discovered which could affect the content, and all legal disclaimers that apply to the journal pertain.

Keywords

abdominal aorta; abdominal aortic aneurysm; asynchronous; blood flow; blood velocity; cardiac; cardiovascular; cross-correlation; desynchronization; ECG gating; elastography; flow pattern; flow velocity; heart; high frame rate; high frequency; high resolution; infarction; left ventricle; mice; myocardial infarction; myocardium; simultaneous imaging; synchronicity; synchronization; synchronous; ultrasound; vascular; vortex; wall motion; wall velocity

INTRODUCTION

The mechanical property and geometry changes as a result of disease may affect both the wall motion and blood flow. The ischemic or infarcted myocardium undergoes insufficient or no active contraction and thereby wall motion abnormalities such as hypokinesis, akinesis, and dyskinesis (Feigenbaum et al. 2005). The ischemia or infarction also affects the pressure and volume of the left ventricle and thus alters the blood velocities and patterns (Rivas et al. 1976). In the case of abdominal aortic aneurysms, a frequently silent and therefore lethal disease of the older population, Brekken et al. found that the local strain values may exceed the circumferential average strain significantly (Brekken et al. 2006). In a mouse model of abdominal aortic aneurysms, the wall motion and pulse wave propagation are spatially nonuniform, probably due to the increased inhomogeneity of mechanical properties (Luo et al. 2009a). *In-vivo* studies also showed the formation of a flow vortex in the abdominal aneurysm (Sugimoto et al. 1994).

The cardiovascular wall motion and blood flow are also coupled and influence one another. Because blood is incompressible, blood flow in the heart chamber or arterial lumen must accompany regional wall motion during the cardiac cycle. It is therefore reasonable to believe that alterations in regional wall motion may have impact on the regional blood flow. By combining left-ventricular color flow with separately performed tissue Doppler imaging in the heart, a strong inverse linear correlation between intra-ventricular blood velocities and tissue velocities from midseptal segment during isovolumic relaxation was reported (Edvardsen et al. 2005). This relationship was also found between the apical septal velocities and the flow (Edvardsen et al. 2005).

In biomechanics, numerous efforts have concentrated on the fluid-solid interaction and coupling (Egelhoff et al. 1999, Krittian et al. 2010, Vappou et al. 2008, Watanabe et al. 2002, Watanabe et al. 2004). The flow-solid interaction (FSI) is a crucial step in biomechanical modeling and couples computational fluid dynamics (CFD) in fluids and finite-element analysis (FEA) in tissues. The fluid and structural mechanics systems are usually coupled at the interface by the kinematic and dynamic conditions, which define the velocity, pressure and/or other parameters of the fluid and structural nodes at the interface to be the same. Simultaneous and registered imaging of both cardiovascular wall motion and blood velocity may contribute to more complete computational models of cardiovascular mechanical and fluid dynamics and increase the understanding of their interaction (Wan et al. 2010, Wise et al. 2005), as well as provide additional diagnostic information.

Different methods, including frequency (or, phase) domain-based tissue Doppler and time (or, spatial) domain-based speckle tracking methods, have been developed and clinically used to estimate the wall motion and deformation of the heart and artery in normal and pathological cases *in vivo* (de Korte et al. 2000, Konofagou et al. 2002, Maurice et al. 2005, Sutherland et al. 2004). On the other hand, blood flow is routinely measured in the clinic. Techniques for blood flow measurement include pulsed Doppler, power Doppler and color flow imaging (i.e., color Doppler), mainly based on estimation of frequency shift or phase shift due to the Doppler effect (Hoskins 1999). In color flow imaging, in addition to the conventional and widely-used frequency domain auto-correlation (Kasai et al. 1985), time domain cross-correlation and other methods have also been developed as alternative approaches, offering aliasing free velocity detection and angle-independent capability (Bonnefous and Pesque 1986, Shariati et al. 1993, Trahey et al. 1987).

Estimation of both the wall motion and blood flow in the carotid artery using ultrasound methods has recently been of clinical interest. In Bambi et al. (2004), two ultrasound beams were separately steered at different angles for the wall and blood; echoes generated from the walls and from the blood were independently processed to obtain both blood flow and wall motion of the common carotid artery, and to further estimate the wall shear strain and distensibility. Tortoli et al. (2006) improved the system by dividing a linear array probe into two subapertures to simultaneously estimate the blood flow and wall motion. Balocco et al. (2010) used the blood flow and wall motion data obtained by this system and estimated the viscoelastic properties of vessel walls. In these approaches, only two M-mode or Doppler beams were considered. In Hasegawa and Kanai (2008), the radial strain of a human carotid arterial wall and blood flow were simultaneously imaged *in vivo* by using ultrasonic radio-frequency (RF) echoes acquired at a high frame rate (about 3500 Hz) with parallel beamforming. Wan et al. (2010) acquired the RF data in a limited field of view at a frame rate of 111 Hz and simultaneously imaged the blood flow, wall motion and strains in the human carotid artery.

In the field of Magnetic resonance imaging (MRI), several methods have been developed to image both the wall motion and blood flow of the hearts. Sampath et al. (2008) obtained simultaneous measurements of one-dimensional (1-D) myocardial displacement and chamber blood flow in normal humans and pathological pigs with moderate ischemic mitral regurgitation, using an MRI technique of spatial modulation of magnetization with encoded gradients for gauging speed. The findings demonstrated multiphase correlated measurements of myocardial motion and chamber blood flow. The obtained myocardial displacement and blood flow may be useful in the planning and evaluation of mitral-valve repair procedures. Wise et al. (2005) estimated simultaneously the blood flow patterns and ventricular wall velocities in the rat heart using phase contrast MRI. The main limitation of the MRI methods lies in the low temporal resolution. Typically, the measurements in Wise et al. (2005) are limited to 12 time points per cardiac cycle.

Mouse models are becoming increasingly popular in cardiovascular research, not only because mice are low-cost and widely available for their easy breeding, short reproductive cycle (about 10 weeks), short time of pregnancy (about 19 days) and numerous offsprings (5-10 newborn mice from one pregnancy), but also because it is now easier to construct

mouse models through genetic modifications (such as gene mutation and knockout), surgery or pharmacologic manipulation (Breslow 1996, Daugherty and Cassis 2004, Tarnavski et al. 2004). In addition, 99% of mouse genes have homologues in man; and many homologous genes have identical functions in mouse and human (Waterston et al. 2002). As a result, anatomy, physiology and metabolism are similar and genetic disease pathology can be very similar (Waterston et al. 2002). Therefore, mouse models are suitable in mimicking human pathological processes.

Echocardiography with 10-15 MHz linear arrays has been used to image the left-ventricular anatomy and assess myocardial function in different mouse models (Derumeaux et al. 2008, Kanno et al. 2002, Patten et al. 1998, Peng et al. 2009, Thibault et al. 2009, Thibault et al. 2007). The small size of mouse tissues (e.g., size of the heart $< 8 \times 6 \text{ mm}^2$, diameter of the abdominal aorta $< 1 \text{ mm}$) and rapid heart rate (300 to 600 bpm) (Wehrens et al. 2000) require an imaging modality with both high temporal and high spatial resolution capability. High-frequency (20-75 MHz), small animal ultrasound systems have recently become commercially available. To overcome frame-rate limitations in high-frequency systems, the retrospective electrocardiogram (ECG) gating and prospective ECG triggering techniques have been developed (Cherin et al. 2006, Ketterling and Aristizabal 2009, Liu et al. 2006). Based on a high frequency (30 MHz) Vevo 770 system (VisualSonics Inc., Toronto, ON, Canada) and the retrospective ECG-gating technique, our laboratory has developed a high-frame-rate (8 kHz) RF data acquisition system (Pernot et al. 2007), which allows us to estimate the minute motion, deformation and rapid wave propagation in the mouse heart (Konofagou et al. 2010, Luo et al. 2007a, Luo and Konofagou 2008, Pernot et al. 2007) and abdominal aorta (Fujikura et al. 2007, Luo et al. 2009a) with simultaneously very high temporal and spatial resolution. Two-dimensional (2-D) speckle tracking on B-mode images at high frame rates (1 kHz) were also used to estimate myocardial motion in mice (Li et al. 2007a), while estimation methods for flow imaging with high frequency ultrasound images were studied in Aoudi et al. (2006) and Marion et al. (2010). Doppler techniques have been used in mice in difference applications (Reddy et al. 2005). Hartley et al. (1995) measured the ascending aortic blood velocity in mice using a 20-MHz pulsed Doppler ultrasound. In a pioneering work, they also obtained Doppler signals simultaneously from both vessel walls of mouse carotid arteries and from blood flow using one or two probes, and estimated the blood velocity, near and far artery wall motion, and net diameter change and wall velocity (Hartley et al. 2004a). In that work, the blood velocity and wall displacement, diameter or velocity waveforms are typically shown (Hartley et al. 2004a).

High-frequency (15-50 MHz) linear-array transducers have recently become commercially available (Vevo 2100, VisualSonics Inc.) (Foster et al. 2009). The linear-array transducers provide uniform high resolution maintained over the full field of view. The Vevo 2100 system provides 2D speckle tracking in the VevoStrain™ software for myocardial wall motion (and deformation) assessment, and color Doppler mode for flow imaging. With these two modes, the wall motion and blood flow could be obtained separately. However, without the use of ECG gating, the frame rate of the 2D data stays below 400-500 Hz for the full view of a mouse left ventricle, which, to our knowledge, may be limited in regard to the

optimal performance of transient motion and deformation analysis in mice (Luo *et al.* 2007b).

The objective of this study to demonstrate the feasibility of imaging wall motion coupled with blood velocity in murine hearts and vessels *in vivo*, which may provide important information for fluid-solid interaction and coupling and for diagnosis of cardiovascular disease.

In this work, we aimed for 2-D imaging of both the wall motion and blood velocity in mice with the use of ECG gating, which provides additional spatial information and may be helpful. The RF data of myocardial wall and heart chamber, or abdominal aortic wall and lumen, were used to estimate both the wall motion and blood flow. Since identical frames of RF data were used, these two measurements were automatically registered, both spatially and temporally. At each lateral location, the two measurements were obtained at the same time (i.e., simultaneously). Due to the use of ECG gating, however, the measurements at different lateral locations were not obtained at the same time. Therefore, throughout this paper, the term “*simultaneous imaging*” used in this study indicates that the same RF data were used to estimate both the wall motion and blood velocity, and these estimates at each lateral location were obtained from the same time.

METHODS

Animal Preparation

Brown C57-BL6 wide-type mice (Charles River Laboratories, Wilmington, MA) were anesthetized with an inhaled mixture of 2% isoflurane (AErrane, Baxter Healthcare Corp., Deerfield, IL) and oxygen (Tech Air of Connecticut, Inc., White Plains, NY) by using an isoflurane vaporizer (Model 100, SurgiVet, Inc., Waukesha, WI), with the approval from the Institutional Animal Care and Use Committee (IACUC) of Columbia University. The hair over the chest or abdomen was removed. The mice were placed supine on a heating platform (THM100, Indus Instruments, Houston, TX, USA) to maintain a constant body temperature (approximately 37 °C). The ultrasound probe was placed on the mouse chest or abdomen using degassed ultrasound gel (Aquasonic 100, Parker Laboratories Inc., Orange, Fairfield, NJ) as a coupling medium. Care was taken to avoid the formation of air bubbles in the gel. The ECG was obtained from the electrode pads on a heating mouse platform (THM100, Indus Instruments, Houston, TX).

In the myocardial infarction (MI) model, an anterolateral and anterior infarct MI was induced through permanent ligation of the left anterior descending (LAD) coronary artery in mice after left-sided thoracotomy (Kumar *et al.* 2005, Tarnavski *et al.* 2004). Mice were initially anesthetized using isoflurane (1-5% mixture with 100% oxygen). After subcutaneous administration of 0.1ml of 0.1% lidocaine, a left thoracotomy was performed in the fourth intercostals space and heart was exposed. Proximal LAD coronary artery was ligated at the site just below the inferior edge of left atrium with use of 8-0 nylon suture. The chest wall was then closed with the interrupted suture of 5-0 silk and skin was closed with continuous suture of 5-0 nylon. The MI mouse was scanned 1 day after ligation.

In the abdominal aortic aneurysm (AAA) model, a subcutaneous osmotic minipump (Alzet model 2004, Durect Corp, Cupertino, CA) was implanted into the mice to deliver a slow release of AngII (1.44mg/kg/day) (Deng *et al.* 2003). The mice were anesthetized with subcutaneous administration of 0.1ml of 0.1% lidocaine. Using sterile techniques, a subcutaneous pocket was created in the back above the scapular region and the osmotic minipump (Alzet model 2004) was then placed in this pocket. These pumps contained Angiotensin II in dosages previously described. The muscles and skin were then closed using 5-0 absorbable and nylon sutures. The mice were scanned 28 days after pump implantation.

RF Data Acquisition

The high frame-rate data acquisition system previously developed (Pernot *et al.* 2007) was used. A 30-MHz ultrasound probe (RMV-707B, VisualSonics Inc., Toronto, ON, Canada) was placed on the mouse chest in the parasternal position to obtain a longitudinal (long-axis) view of the LV of the heart, or on the abdomen to obtain a long-axis view of the abdominal aorta in the suprarenal region. The field of view was equal to 12×12 mm², the axial and lateral image resolutions of the probe (30-MHz) were equal to 55 and 115 μ m, respectively. In the EKV (ECG-based kilohertz visualization) mode provided by the imaging system (Vevo 770, VisualSonics Inc.), the transducer worked on a line-by-line basis (i.e., multiple M-mode). The transducer transmitted and received at a pulse-repetition frequency (PRF) of 8 kHz at each position of the transducer. The data acquisition was triggered by the synchronization signal of RF lines, which indicated when the transducer transmitted the ultrasonic pulses. A two-channel, 14-bit waveform digitizer (CompuScope 14200, Gage Applied Technologies Inc., Lachine, QC, Canada) was used to simultaneously acquire the RF signals of the ultrasound transducer and the associated ECG at 200 MHz and 8 kHz, respectively. 180-192 lines were acquired over the entire field of view. Each acquisition lasted approximately 7 min. After data acquisition, the acquired RF signals were gated between two consecutive R-waves in the ECG to reconstruct the RF image sequence for a complete cardiac cycle at the extremely high frame rate of 8 kHz (Luo *et al.* 2007a, Luo and Konofagou 2008, Pernot *et al.* 2007). The reader is referred to previous work (Luo *et al.* 2007a, Luo *et al.* 2009a, Luo and Konofagou 2008, Pernot *et al.* 2007) for further details of the data acquisition protocol.

Six (n=6) normal hearts, five (n=5) infarcted hearts, five (n=5) normal aortas and four (n=4) aneurysmal aorta were chosen from our database. Two main criteria were used for the selection of the datasets. First, the angles between the radial direction of the heart/aorta and the axial direction of the ultrasound beam was approximately 10-20 degrees, thus allowing for the estimation of both wall motion and blood velocity, as will be discussed later. Secondly, the echogenicity in the heart chambers or aortic lumen should be high enough for the blood velocity estimation using the speckle tracking method. The sonographic signal-to-noise ratio in the blood is typically very low. The datasets with relatively high signal intensities in the blood were included in the sample selected. In addition, the B-mode cine-loop was used to define the timing of the mitral valve opening or aortic valve opening. Therefore, another criterion for the data selection was the appearance of the valves.

Wall Motion and Blood Flow Estimation

The axial wall velocity of the myocardium or aortic wall and blood velocity in the left ventricle chamber or aortic lumen were estimated off-line from the same RF data acquired, using a time-efficient 1-D normalized cross-correlation technique previously described (Luo and Konofagou 2010). The window size was equal to 480 μm , and the window overlap was equal to 95%. The wall velocity and blood velocity estimates were minimally smoothed by a 3×3 median filter in order to remove the peak hopping errors in speckle tracking. The rigid motion induced by respiration was removed by subtracting the velocity of the surrounding tissue above the wall from the velocity of the wall and blood.

Both the wall velocity and blood velocity were color-coded and superimposed onto the grayscale B-mode images using an overlay blending mode (Bunks 2000). Due to the significant difference between the wall and blood velocity ranges, the scale of the blood velocity data was 10 and 40 times higher than that of the wall velocity data in the heart and aorta, respectively.

RESULTS

Heart

Figure 1 depicts the 2-D images of wall velocity and blood velocity of a normal and an infarcted heart in the systolic phase after the aortic valve opens. The wall velocity in the apical region of the infarcted hearts is shown significantly lower, due to the apical infarction (Luo *et al.* 2007a). The flow near the basal region and the aorta is consistently negative or positive for the normal and infarcted cases, respectively. Considering the orientation of the heart in the images and the location of the aortic valve, these results demonstrate that the flow is directed to the aortic valve in both cases, in accordance with the systolic phase. The flow near the apical region of the infarcted heart is smaller, mostly likely due to the angle dependence of this study.

Figure 2 shows the 2-D images of wall velocity and blood velocity in a normal heart during the diastole (a) before and (b-d) immediately after the mitral valve opens, i.e., during the isovolumic relaxation and rapid ventricular filling phases, respectively. The timing of the mitral valve opening was determined by carefully observing the B-mode cine-loop (video_1.avi). Before the mitral wave opens, both the wall velocity and blood velocity are relatively small (a). After the mitral wave opens (c-d), the blood moves from the left atrium to the left ventricle while the left-ventricular myocardium relaxes. Therefore, both the wall velocity and flow increase rapidly, as shown in (c-d). Fig. 2(d) also shows a negative flow region in the middle of the chamber, opposite from the strong positive flow near the basal level. This may suggest the formation of a flow vortex, which is confirmed on the B-mode cineloop. The formation of a vortex in the diastolic phase can increase the efficiency of the fast filling phase (Gharib *et al.* 2006, Krueger and Gharib 2003).

Figure 3 depicts the 2-D images of wall velocity and blood velocity in an infarcted heart during the diastole, (a) before and (b-d) immediately after the mitral valve opens, i.e., isovolumic relaxation and rapid ventricular filling phases, respectively. The timing of the mitral valve opening was determined by the B-mode cine-loop (video_2.avi). Similar to the

normal case, the blood velocity is relatively low before the mitral valve opens. Both the flow and wall velocity increase after the mitral valve opens. The opposite flow near the basal and apical region also suggests the formation of a flow vortex. Similar to the systolic phase (Fig. 1), the wall velocity in the apical region is shown significantly lower in the infarcted hearts (Fig. 3) than in the normal heart (Fig. 2). In Fig. 3(a), however, the wall motion near the base is relatively high, compared with the flow, although the valve is still closed. This indicates that the increased wall motion occurs earlier than the increased flow in the infarcted case.

Figure 4 shows the M-mode images of wall velocity and blood velocity of the (a) normal and (b) infarcted hearts. The M-mode data were acquired in the locations near the mitral valve indicated by the dashed line in Figs. 2 and 3. In the normal case (Fig. 4(a)), both the wall velocity and blood velocity increase in the rapid filling phase (i.e., after the mitral valve opens). In other words, the wall motion and blood flow are synchronized in the diastolic phase. In the infarcted case (Fig. 4(b)), however, the wall velocity starts increasing before the mitral valve opens (i.e., isovolumic relaxation phase) while the blood velocity starts increasing after the mitral valve opens (i.e., rapid filling phase). The time delay between the blood velocity and wall velocity onsets was approximately 20 ms. This phenomenon is also confirmed in another 5 normal and 4 infarcted hearts. In the normal (n=6) and infarcted (n=5) hearts, the time delays were 0.3 ± 0.8 ms and 21.2 ± 1.9 ms (mean \pm standard deviation), respectively. A significant difference ($p < 0.001$) was found between normal (n=6) and infarcted (n=5) hearts.

Figure 5 illustrates the M-mode images of the correlation coefficients in the motion estimation of the (a) normal and (b) infarcted hearts. As shown, the correlation in the wall is significantly higher than that in the chamber. The correlation of the chamber is the lowest in the rapid filling phase, due to the highest blood velocity. The correlation coefficient is mostly higher than 0.95 and 0.85 in the wall and chamber of the normal heart, respectively. The correlation coefficient is mostly higher than 0.9 in the wall of the infarcted heart, and is lower but still higher than 0.5 in the chamber.

Aorta

Figure 6 depicts the 2-D images of the wall velocity and blood velocity of the normal suprarenal abdominal aorta during the propagation of the pulse wave (Luo *et al.* 2009a) in the systolic phase. After the aortic valve opens, the blood is ejected from the left ventricle into the aorta. As a result, both the blood velocity and the diameter of the lumen increase. As shown, the wall motion and blood velocity are synchronized. The low blood velocity near the rightmost and leftmost regions is mainly due to the angle dependence of the method.

Figure 7 illustrates the wall and blood velocity waveforms of the normal aorta over one cardiac cycle (from ECG R-wave peak to the next R-wave peak). The waveforms correspond to the regions indicated by circles in Fig. 6(d). The waveforms of the wall velocity and blood velocity are similar to some extent. In particular, the temporal onsets of the wall motion and blood velocity increase are identical. The synchronization between wall velocity and blood velocity was found in another four normal aortas. The temporal location

of the maximum wall velocity occurs earlier than that of the maximum blood velocity, which is in agreement with the data shown in Hartley et al. (2004b).

Figure 8 shows the 2-D images of wall velocity and blood velocity of the aneurysmal suprarenal abdominal aorta. In accordance with our previous results (Luo *et al.* 2009a), the wall velocity in the aneurysmal aorta is lower than and not as uniform as in the normal case, probably due to the regional stiffening and increased inhomogeneities of the wall properties and geometry. The flow and the thrombus observed in the proximal region of the aneurysm sac may also have influenced the wall motion. Opposite flow patterns are found in the sac of the aneurysm, which may suggest the formation of a flow vortex, also confirmed on the B-mode cineloop.

Figure 9 compares the wall and blood velocity waveforms of the aneurysmal aortas in one cardiac cycle. The waveforms are taken from the regions indicated by circles in Fig. 8(d). Unlike in the normal case, the wall motion and blood velocity in the aneurysmal case are not synchronized. It appears that the onset of the wall motion occurs 7 ms earlier than that of the blood velocity. The synchronicity between wall velocity and blood velocity waveforms is significantly reduced in the aneurysmal case than in the normal case. In addition, the negative flow of the distal region (Fig. 8) may suggest the formation of a flow vortex inside the saccular region of the aneurysm. The asynchrony between wall velocity and blood velocity as well as opposite flow patterns was found in another three aneurysmal aortas. The delays between wall velocity and blood velocity onsets were 1.2 ± 0.5 ms and 8.2 ± 2.6 ms (mean \pm standard deviation) in the normal (n=5) and aneurysmal (n=4) aortas, respectively. A significant difference ($p < 0.001$) was found between normal (n=5) and infarcted (n=4) aortas.

DISCUSSION

In this paper, both the wall motion and blood velocity of the mouse left ventricle and abdominal aorta were imaged using cross-correlation on ultrasound RF data acquired at high frame rates. These data may be used as initial input or used to validate the simulation results of biomechanical models with wall-flow interaction, as opposed to exclusive models of either blood flow or wall motion.

In addition to information provided by either wall motion or blood velocity alone, images of both may provide complementary information for diagnosis. Different results were shown in normal and pathological cases in this study. The time delay between the onsets of the wall motion and the blood velocity in the heart (Fig. 4) may indicate the presence of a myocardial infarction. In the infarcted heart, the remote myocardium near the base may need to undergo larger motion in the systolic phase in order to compensate for the low contractility of the infarct (as shown in the M-mode image in Figs. 4(b), compared with Fig. 4(a)). The remote myocardium may thus be in an unsteady state in diastole and reduce the coupling between the wall motion and the blood flow. These diastolic phenomena represent a sudden localized outward motion of a portion of the left ventricular wall that has been observed to occur during the isovolumic relaxation phase of the cardiac cycle, as known as segmental early relaxation or asynchronous relaxation (Gaasch et al. 1985). The B-mode cineloop and blood

velocities were used to determine the isovolumic relaxation and rapid filling, while the delay between the wall motion and blood velocities confirm these asynchronous relaxation phenomena. Therefore, imaging of both the wall motion and the blood velocity provides a unique opportunity to investigate such phenomena and other abnormalities.

The similarity between the wall velocity and blood velocity waveforms in the normal aorta (Fig. 7) lies in the fact that both are related to the pressure. Wall velocity is related to the time derivative of pressure while blood velocity is related to the spatial derivative of pressure along the vessel (Nichols and O'Rourke 2005). In the normal aorta where the vessel geometry and mechanical properties are relatively uniform, these two derivatives were somehow dependent. Due to this similarity, as suggested by Hartley et al. (2004b), the potential exists to use velocity in place of flow (and diameter in place of pressure) to study arterial mechanics, vascular impedance and wave reflections in mice. Further studies with simulations should be performed in order to better unveil the underlying mechanisms.

The asynchrony between the wall motion and blood flow may also suggest abnormality in the aorta. The results of vortex formation and location were in good agreement with simulation results (Taylor and Yamaguchi 1994), experimental results in the abdominal aortic aneurysm models of straight tubes with an asymmetric bulge (Yu 2000, Yu and Zhao 2000) and *in-vivo* results in humans (Sugimoto *et al.* 1994). The coupling between the wall and the flow is weaker in the AAA, i.e., their onsets were not registered temporally, probably due to inhomogeneous wall properties and geometry as well as complex flow patterns. Imaging of both wall motion and blood velocity may thus provide further insight in the complex nature of AAA, in particular, in the interaction between wall and flow.

A critical requirement of imaging of both the wall motion and blood velocity is acquisition of the high-frame rate data. In Doppler-based or frequency-domain methods, a minimum pulse repetition frequency (PRF), which is equivalent to the frame rate for data processing, is required to avoid phase aliasing and thus to allow for accurate estimation of high blood velocities. In color flow imaging and other Doppler techniques, the PRF is typically on the order of a few kilohertz. It is worth mentioning that the PRF used for both human and mouse is on the same order, probably due to similar range of maximum blood velocity (on the order of 10-100 cm/s). In time-domain methods such as speckle tracking, a high frame rate can increase the similarity between consecutive frames or correlation coefficient in motion estimation. We previously showed that frame rates between 2000-2700 Hz were optimum for strain estimation of the murine hearts (Luo et al. 2007b). In this paper, the frame rate of 8 kHz was used for wall motion and blood velocity estimation in the murine hearts and aortas, thus meeting the requirement of speckle tracking for both wall and blood flow.

Only the axial component of the myocardial motion and blood velocity was estimated in this study. Difficulties were identified for 2-D speckle tracking in conjunction with the ECG gating used, as previously discussed (Luo and Konofagou 2008). Hearts typically undergo complicated motion in the three-dimensional (3-D) space. The long-axis view was used because the axial aligned with the radial direction in most of the myocardium except at the apex. However, the direction of the blood flow does not necessarily coincide with the axial direction of the ultrasound beam. Similarly, the radial motion of the aorta is approximate to

the axial direction of ultrasound in the long axis view. In addition to the radial motion, the aorta may also undergo longitudinal or out-of-plane motion. However, the direction of the blood flow is mainly along the longitudinal direction of the aorta, closer to the lateral direction of ultrasound. In this study, in order to image both the wall motion and blood flow, the ultrasound incident angle of the datasets chosen was approximately 10-20 degrees between the radial direction of the heart/aorta and the axial direction of the probe. Due to the incident angle, both the wall velocity and blood velocity were underestimated in this study, especially the blood velocity. In this study, however, the timing of the wall motion and blood velocity is more important than the accurate magnitude, since the synchronicity or coupling between the two is of interest.

The 1D time-domain estimation method used in this work suffers from the same angle dependence as that of Doppler methods. However, Doppler-based methods typically use small-bandwidth signals and therefore have the disadvantage of low axial resolution. Spatial resolution can be improved with shorter and wider-bandwidth transmit pulses, but usually at the cost of less precise Doppler spectra (Hartley *et al.* 2004b, Newhouse *et al.* 1980). In addition, our method generates 2D images of both wall motion and flow velocity, which provide additional spatial information.

In order to confirm the presence of a flow vortex, 2-D motion is necessary to calculate the vorticity, as was done in the literature (Faludi *et al.* 2010, Hong *et al.* 2008, Kheradvar *et al.* 2010). In this study, opposite flow patterns were found in both normal and infarcted hearts as well as the aneurysmal aorta. Due to the use of 1-D motion estimation in this study, the opposite flows could be the 1-D projection of a flow vortex. Therefore, these may suggest the formation of a flow vortex, which was also confirmed on the B-mode cine loop. The vortex will be validated in the future, once accurate 2-D motion estimation is accomplished.

The correlation coefficient in the lumen was found to be lower than in the myocardium (Fig. 5) and in the aortic wall (not shown). This can be explained by three reasons. First, the blood velocity is much higher than the wall motion. At the same frame rate, the inter-frame speckle motion is thus much higher in the blood, resulting in thus the high decorrelation. A frame rate of 8000 Hz is deemed sufficient for the wall motion estimation. However, the flow may require a higher frame rate for the best estimation quality, especially in the rapid filling phase. Second, as mentioned above, only 1-D motion estimation was used in this study. The lateral motion further reduces the correlation, especially in the flow, where the lateral component was much more significant due to the angle used (approximately 10-20 degrees). Third, the sonographic signal-to-noise ratio (SNR) is much lower in the blood than in the tissue, due to less ultrasound scatterers in the blood.

A potential method to increase the SNR is to use contrast agents. Contrast agents have been used to improve the quality of blood flow imaging in echo-particle image velocimetry (Echo-PIV) (Faludi *et al.* 2010, Kheradvar *et al.* 2010, Sengupta *et al.* 2007). Echo PIV typically uses B-mode data to estimate the blood flow. The use of RF signal instead of B-mode data provides high spatial resolution and higher precision in the estimation (Walker and Trahey 1994). The frame rate of the Echo PIV data is also limited (usually < 100 Hz). In the future, contrast agents will be used to enhance the SNR in the blood lumen as well as in

the wall. The image intensity enhancement from the contrast agents lasts more than 11 minutes (Li *et al.* 2007b), the use of ECG gating (2-7 minutes) should not be a major problem.

The wall motion and blood velocity in different cardiac phases in diastole (such as early diastole and late diastole) vary, as partially shown in the M-mode images (Fig.4). In this feasibility study, we have mainly investigated the early diastolic phase. However, comparison of different diastolic phases is of interest in future studies.

This is a feasibility study of imaging both wall motion and flow velocity with a limited number of mice and two opposite cases (i.e., normal vs. infarcted hearts with permanent LAD ligation, and normal aorta vs. aneurysmal aorta after 28 days Ang II infusion). Preliminary statistical analysis was performed on normal (n=6) and infarcted (n=5) hearts, and normal (n=5) and aneurysmal (n=4) aortas, with significant differences ($p < 0.001$) found in both cases. In the present study, intact mice were used as controls; sham procedures were not included. An ideal study design requires the use of a group of sham-operated mice in order to eliminate the effects of the surgery. In the case the left ventricle, the murine chest can be opened and then closed, without ligating the LAD coronary artery. In the case of abdominal aorta, mice can receive phosphate buffered saline instead of AngII. In our previous study (Luo *et al.* 2009a), no significant difference in wall motion was found between intact and sham mice. In the future, once the acquisition method is optimized, we will test the methodology on a larger population. A follow-up study after myocardial infarction in mice could be performed in the future to investigate the wall motion and blood velocity change over time after left ventricular remodeling. The occlusion and reperfusion of the coronary artery could also be used to generate more complex disease models like acute ischemia and its recovery. The wall motion and blood velocity will be imaged in such models in the future. Barisione *et al.* (2006) have shown that AngII infusion led to rapid dilation of suprarenal aortas during the initial 7 days of infusion in male apolipoprotein E (ApoE) $-/-$ mice. Our ongoing work also includes the longitudinal study of the mice after AngII infusion to investigate the change of the wall motion and blood velocity during the progression of the aneurysm.

In this study, arterial wall velocity was estimated. Wall velocity is similar to the temporal derivative of the blood pressure (dp/dt) (Hartley *et al.* 2004b). Wall velocity waveform can be integrated to generate the wall displacement and diameter waveforms, which closely resemble the blood pressure waveform (P) (Hartley *et al.* 2004b). Many potentially useful vascular indices (e.g., wave intensity, wave reflection augmentation index and vascular impedance) can be generated from the vessel diameter, and similarly, from blood velocity signals (Hartley *et al.* 2004b). The estimates of these vascular indices from the diameter waveform and blood velocity could be compared in both normal and aneurysmal aortas, and validated against those estimated from pressure measurements.

The retrospective ECG gating techniques rely on the periodicity of the ECG signal. As such, arrhythmia could potentially limit their use. In the data acquisition, efforts were made in maintaining the temperature and monitoring the heart rate of the mouse. In the data processing, the ECG associated with each RF line was also analyzed. The data were rejected

if the heart rate or the ECG waveform varied significantly (Cherin *et al.* 2006). For the purpose of this study, ECG gating also requires that the wall motion and blood velocity are periodic. Pre-ejection times of mouse hearts, from the onset of electrical ventricular stimulation to the aortic opening, ranged from 10 to 20 ms, depending on the mouse strain, the anesthetic used and the temperature (Hartley *et al.* 1995, Williams *et al.* 2007). Pre-ejection time can vary from one heartbeat to the other in mice by as much as 1 ms. With the use of ECG gating, only physiologic states with long-term stability can be assessed. For each ultrasound line, the temporal resolution is 125 μm , given the frame rate used (8 kHz). However, long acquisition times (7 min in this paper) may affect the temporal resolution. Irregular flow patterns may not be identical across cardiac cycles. The flow velocity images in Figs. 6 and 8 as well as flow velocity videos (not shown) demonstrate strong coherence along the lateral direction and over time, although a minimal spatial filtering and no temporal filtering were used. Variations of flow patterns (and wall motion) over different cardiac cycles would manifest as random noise on the 2-D images and would not be identifiable on the images.

For the purpose of this feasibility study, only the wall velocity was considered. Wall motion (displacement and velocity) estimates cannot differentiate between active contraction and simple rotation or translation of the heart, or between passive tethering and active contraction. Previous studies have shown that myocardial elastography, a cardiac strain estimation method, can accurately characterize normal myocardial function throughout an entire cardiac cycle as well as detect and localize myocardial infarction *in vivo* (Luo *et al.* 2007a). In the future, myocardial deformation (i.e., strain and strain rate) could be combined with blood velocity estimation. However, the estimates of wall motion in this study and deformation in previous studies (Luo *et al.* 2007a) still suffer from the 1-D estimation used. 2-D strain estimation is often used to overcome this limitation (Jia *et al.* 2009, Lee *et al.* 2007, Li *et al.* 2007a, Luo *et al.* 2009b). 2-D speckle tracking methods, mostly based on B-mode images, have been commercially available in the clinic.

The mechanical scanner and ECG gating used in this paper sacrifices many of those potential advantages of simultaneous imaging of both wall motion and blood flow. These methods are useful mainly with the older Vevo 770 system, which is still used by many cardiovascular research laboratories. For human applications, imaging of both the wall motion and blood flow could be obtained by acquiring high frame-rate data from a phase array and with ECG gating (Wang *et al.* 2008).

CONCLUSIONS

Cardiovascular wall motion and blood flow and their respective coupling were both imaged in mice *in vivo*. Distinct results were found between normal and infarcted hearts, and between normal and aneurysmal aortas. In contrast to the synchronized wall motion and blood velocity in the normal heart, time delay between wall motion and blood velocity were found in the infarcted heart in the diastolic phase, i.e., the wall motion and blood velocity occurred in the isovolumic relaxation and rapid filling phases, respectively. In the aneurysmal aorta, opposite flow patterns were depicted in the saccular region, suggesting the formation of a flow vortex. The wall motion and blood velocities in the aneurysmal aorta

were found to be less synchronized than in the normal case. Imaging of both wall motion and blood velocity may thus provide important insight for the diagnosis of cardiovascular disease as well as essential parameters for biomechanical modeling of the fluid-solid interaction between the blood dynamics and the cardiovascular wall mechanics.

Supplementary Material

Refer to Web version on PubMed Central for supplementary material.

Acknowledgments

This work was supported in part by NIH R01EB006042 and R01HL098830. The authors wish to express their sincere thanks to Kana Fujikura, M.D., Ph.D., in the Department of Biomedical Engineering of Columbia University, for performing the echocardiography scans, Iwao Matsunaga, M.D., in the Department of Surgery of Columbia University, for performing LAD ligation in mice, Leslie S. Tyrie, M.D., and M. David Tilson, M.D., in St. Luke's-Roosevelt Hospital Center, for creating the mouse model of AAA, Jonathan Vappou, Ph.D., in the Department of Biomedical Engineering of Columbia University, for helpful discussion and Shunichi Homma, M.D., in the Department of Medicine of Columbia University, for kindly allowing access to the ultrasound system used for the experiments.

REFERENCES

- Aoudi W, Liebgott H, Needles A, Yang V, Foster FS, Vray D. Estimation methods flow imaging with high frequency ultrasound. *Ultrasonics*. 2006; 44:E135–E140. [PubMed: 16844170]
- Balocco S, Basset O, Courbebaisse G, Boni E, Frangi AF, Tortoli P, Cachard C. Estimation of the viscoelastic properties of vessel walls using a computational model and Doppler ultrasound. *Phys. Med. Biol.* 2010; 55:3557–3575. [PubMed: 20508319]
- Bambi G, Morganti T, Ricci S, Boni E, Guidi F, Palombo C, Tortoli P. A novel ultrasound instrument for investigation of arterial mechanics. *Ultrasonics*. 2004; 42:731–737. [PubMed: 15047375]
- Barisione C, Charnigo R, Howatt DA, Moorleghen JJ, Rateri DL, Daugherty A. Rapid dilation of the abdominal aorta during infusion of angiotensin II detected by noninvasive high-frequency ultrasonography. *J. Vasc. Surg.* 2006; 44:372–376. [PubMed: 16890871]
- Bonnefous O, Pesque P. Time domain formulation of pulse-doppler ultrasound and blood velocity estimation by cross-correlation. *Ultrason. Imaging*. 1986; 8:73–85. [PubMed: 2946098]
- Brekken R, Bang J, Odegard A, Aasland J, Hernes TAN, Myhre HO. Strain estimation in abdominal aortic aneurysms from 2-D ultrasound. *Ultrasound Med. Biol.* 2006; 32:33–42. [PubMed: 16364795]
- Breslow JL. Mouse models of atherosclerosis. *Science*. 1996; 272:685–688. [PubMed: 8614828]
- Bunks, C. *Grokking the GIMP*. Sams Publishing; Indianapolis, IN: 2000. (available at <http://gimp-savvy.com/BOOK/index.html>)
- Cherin E, Williams R, Needles A, Liu GW, White C, Brown AS, Zhou YQ, Foster FS. Ultrahigh frame rate retrospective ultrasound microimaging and blood flow visualization in mice in vivo. *Ultrasound Med. Biol.* 2006; 32:683–691. [PubMed: 16677928]
- Daugherty A, Cassis LA. Mouse models of abdominal aortic aneurysms. *Arterioscler. Thromb. Vasc. Biol.* 2004; 24:429–434. [PubMed: 14739119]
- de Korte CL, Pasterkamp G, van der Steen AFW, Woutman HA, Bom N. Characterization of plaque components with intravascular ultrasound elastography in human femoral and coronary arteries in vitro. *Circulation*. 2000; 102:617–623. [PubMed: 10931800]
- Deng GG, Martin-McNulty B, Sukovich DA, Freay A, Halks-Miller M, Thinnis T, Loskutoff DJ, Carmeliet P, Dole WP, Wang YX. Urokinase-type plasminogen activator plays a critical role in angiotensin II-induced abdominal aortic aneurysm. *Circ.Res.* 2003; 92:510–517. [PubMed: 12600880]
- Derumeaux G, Ichinose F, Raher MJ, Morgan JG, Coman T, Lee C, Cuesta JM, Thibault H, Bloch KD, Picard MH, Scherrer-Crosbie M. Myocardial alterations in senescent mice and effect of

- exercise training a strain rate imaging study. *Circ.- Cardiovasc. Imaging*. 2008; 1:227–234. [PubMed: 19808547]
- Edvardsen T, Rodevand O, Endresen K, Ihlen H. Interaction between left ventricular wall motion and intraventricular flow propagation in acute and chronic ischemia. *Am. J. Physiol.-Heart Circul. Physiol.* 2005; 289:H732–H737.
- Egelhoff CJ, Budwig RS, Elger DF, Khraishi TA, Johansen KH. Model studies of the flow in abdominal aortic aneurysms during resting and exercise conditions. *J. Biomech.* 1999; 32:1319–1329. [PubMed: 10569710]
- Faludi R, Szulik M, D'Hooge J, Herijgers P, Rademakers F, Pedrizzetti G, Voigt JU. Left ventricular flow patterns in healthy subjects and patients with prosthetic mitral valves: An in vivo study using echocardiographic particle image velocimetry. *J. Thorac. Cardiovasc. Surg.* 2010; 139:1501–1510. [PubMed: 20363003]
- Feigenbaum, H.; Armstrong, WF.; Ryan, T. *Feigenbaum's Echocardiography*. Lippincott Williams & Wilkins; Philadelphia, PA: 2005.
- Foster FS, Mehi J, Lukacs M, Hiron D, White C, Chaggares C, Needles A. a new 15-50 MHz array-based micro-ultrasound scanner for preclinical imaging. *Ultrasound Med. Biol.* 2009; 35:1700–1708. [PubMed: 19647922]
- Fujikura K, Luo J, Gamarnik V, Pernot M, Fukumoto R, Tilson MD, Konofagou EE. A novel noninvasive technique for pulse-wave Imaging and characterization of clinically-significant vascular mechanical properties in vivo. *Ultrason. Imaging*. 2007; 29:137–154. [PubMed: 18092671]
- Gaasch WH, Blaustein AS, Bing OHL. Asynchronous (segmental early) relaxation of the left-ventricle. *J. Am. Coll. Cardiol.* 1985; 5:891–897. [PubMed: 3882815]
- Gharib M, Rambod E, Kheradvar A, Sahn DJ, Dabiri JO. Optimal vortex formation as an index of cardiac health. *Proc. Natl. Acad. Sci. U. S. A.* 2006; 103:6305–6308. [PubMed: 16606852]
- Hartley CJ, Michael LH, Entman ML. Noninvasive measurement of ascending aortic blood velocity in mice. *Am. J. Physiol.-Heart Circul. Physiol.* 1995; 268:H499–H505.
- Hartley CJ, Reddy AK, Madala S, Entman ML, Michael LH, Taffet GE. Noninvasive ultrasonic measurement of arterial wall motion in mice. *Proc. IEEE EMBS*. 2004a:3688–3691.
- Hartley CJ, Reddy AK, Madala S, Entman ML, Michael LH, Taffet GE. Noninvasive ultrasonic measurement of arterial wall motion in mice. *Am. J. Physiol.-Heart Circul. Physiol.* 2004b; 287:H1426–H1432.
- Hasegawa H, Kanai H. Simultaneous imaging of artery-wall strain and blood flow by high frame rate acquisition of RF signals. *IEEE Trans. Ultrason. Ferroelectr. Freq. Control*. 2008; 55:2626–2639. [PubMed: 19126487]
- Hong GR, Pedrizzetti G, Tonti G, Li P, Wei Z, Kim JK, Baweja A, Liu SZ, Chung N, Houle H, Narula J, Vannan MA. Characterization and quantification of vortex flow in the human left ventricle by contrast echocardiography using vector particle image velocimetry. *JACC-Cardiovasc. Imag.* 2008; 1:705–717.
- Hoskins PR. A review of the measurement of blood velocity and related quantities using Doppler ultrasound. *Proc. Inst. Mech. Eng. Part H-J. Eng. Med.* 1999; 213:391–400.
- Jia CX, Olafsson R, Kim K, Koliass TJ, Rubin JM, Weitzel WF, Witte RS, Huang SW, Richards MS, Deng CX, O'Donnell M. Two-dimensional strain imaging of controlled rabbit hearts. *Ultrasound Med. Biol.* 2009; 35:1488–1501. [PubMed: 19616362]
- Kanno S, Lerner DL, Schuessler RB, Betsuyaku T, Yamada KA, Saffitz JE, Kovacs A. Echocardiographic evaluation of ventricular remodeling in a mouse model of myocardial infarction. *J. Am. Soc. Echocardiogr.* 2002; 15:601–609. [PubMed: 12050601]
- Kasai C, Namekawa K, Koyano A, Omoto R. Real-time two-dimensional blood-flow imaging using an auto-correlation technique. 1985; 32:458–464.
- Ketterling JA, Aristizabal O. Prospective ECG-gated mouse cardiac imaging with a 34-MHz annular array transducer. *IEEE Trans. Ultrason. Ferroelectr. Freq. Control*. 2009; 56:1394–1404. [PubMed: 19574150]
- Kheradvar A, Houle H, Pedrizzetti G, Tonti G, Belcik T, Ashraf M, Lindner JR, Gharib M, Sahn D. Echocardiographic particle image velocimetry: A novel technique for quantification of left

- ventricular blood vorticity pattern. *J. Am. Soc. Echocardiogr.* 2010; 23:86–94. [PubMed: 19836203]
- Konofagou EE, D'hooge J, Ophir J. Myocardial elastography - A feasibility study in vivo. *Ultrasound Med. Biol.* 2002; 28:475–482. [PubMed: 12049961]
- Konofagou EE, Luo J, Saluja D, Cervantes DO, Coromilas J, Fujikura K. Noninvasive electromechanical wave imaging and conduction-relevant velocity estimation in vivo. *Ultrasonics.* 2010; 50:208–215. [PubMed: 19863987]
- Krittian S, Schenkel T, Janoske U, Oertel H. Partitioned fluid-solid coupling for cardiovascular blood flow: Validation study of pressure-driven fluid-domain deformation. *Ann. Biomed. Eng.* 2010; 38:2676–2689. [PubMed: 20361259]
- Krueger PS, Gharib M. The significance of vortex ring formation to the impulse and thrust of a starting jet. *Phys. Fluids.* 2003; 15:1271–1281.
- Kumar D, Hacker TA, Buck J, Whitesell LF, Kaji EH, Douglas PS, Kamp TJ. Distinct mouse coronary anatomy and myocardial infarction consequent to ligation. *Coronary Artery Dis.* 2005; 16:41–44.
- Lee W-N, Ingrassia CM, Fung-Kee-Fung SD, Costa KD, Holmes JW, Konofagou EE. Theoretical quality assessment of myocardial elastography with in vivo validation. *IEEE Trans. Ultrason. Ferroelectr. Freq. Control.* 2007; 54:2233–2245. [PubMed: 18051158]
- Li Y, Garson CD, Xu Y, Beyers RJ, Epstein FH, French BA, Hossack JA. Quantification and MRI validation of regional contractile dysfunction in mice post myocardial infarction using high resolution ultrasound. *Ultrasound Med. Biol.* 2007a; 33:894–904. [PubMed: 17434660]
- Li Y, Garson CD, Xu YQ, French BA, Hossack JA. Improved myocardial motion tracking in mouse echocardiography using large-diameter microbubbles. *Proc. IEEE Ultrason. Symp.* 2007b:892–895.
- Liu JH, Jeng GS, Wu TK, Li PC. ECG triggering and gating for ultrasonic small animal imaging. *IEEE Trans. Ultrason. Ferroelectr. Freq. Control.* 2006; 53:1590–1596. [PubMed: 16964909]
- Luo J, Fujikura K, Homma S, Konofagou EE. Myocardial elastography at both high temporal and spatial resolution for the detection of infarcts. *Ultrasound Med. Biol.* 2007a; 33:1206–1223. [PubMed: 17570577]
- Luo J, Fujikura K, Tyrie LS, Tilson MD, Konofagou EE. Pulse wave imaging of normal and aneurysmal abdominal aortas in vivo. *IEEE Trans. Med. Imaging.* 2009a; 28:477–486. [PubMed: 19272985]
- Luo J, Konofagou EE. High-frame rate, full-view myocardial elastography with automated contour tracking in murine left ventricles in vivo. *IEEE Trans. Ultrason. Ferroelectr. Freq. Control.* 2008; 55:240–248. [PubMed: 18334330]
- Luo J, Konofagou EE. A fast normalized cross-correlation method for motion estimation. *IEEE Trans. Ultrason. Ferroelectr. Freq. Control.* 2010; 57:1347–1357. [PubMed: 20529710]
- Luo J, Lee W-N, Konofagou EE. Fundamental Performance Assessment of 2-D myocardial elastography in a phased-array configuration. *IEEE Trans. Ultrason. Ferroelectr. Freq. Control.* 2009b; 56:2320–2327. [PubMed: 19942518]
- Luo J, Lee W-N, Wang S, Konofagou EE. An in-vivo study of frame rate optimization for myocardial elastography. *Proc. IEEE Ultrason. Symp.* 2007b:1933–1936.
- Marion A, Aoudi W, Basarab A, Delachartre P, Vray D. Blood flow evaluation in high-frequency, 40 MHz imaging: A comparative study of four vector velocity estimation methods. *Ultrasonics.* 2010; 50:683–690. [PubMed: 20153008]
- Maurice RL, Daronat M, Ohayon J, Stoyanova E, Foster FS, Cloutier G. Non-invasive high-frequency vascular ultrasound elastography. *Phys. Med. Biol.* 2005; 50:1611–1628. [PubMed: 15798347]
- Newhouse VL, Furgason ES, Johnson GF, Wolf DA. The dependence of ultrasound doppler bandwidth on beam geometry. *IEEE Transactions on Sonics and Ultrasonics.* 1980; 27:50–59.
- Nichols, WW.; O'Rourke, MF. McDonald's blood flow in arteries: Theoretical, experimental and clinical principles. Oxford University Press; New York, NY: 2005.
- Patten RD, Aronovitz MJ, Deras-Mejia L, Pandian NG, Hanak GG, Smith JJ, Mendelsohn ME, Konstam MA. Ventricular remodeling in a mouse model of myocardial infarction. *Am. J. Physiol.-Heart Circul. Physiol.* 1998; 274:H1812–H1820.

- Peng Y, Popovic ZB, Sopko N, Drinko J, Zhang Z, Thomas JD, Penn MS. Speckle tracking echocardiography in the assessment of mouse models of cardiac dysfunction. *Am. J. Physiol.-Heart Circul. Physiol.* 2009; 297:H811–H820.
- Pernot M, Fujikura K, Fung-Kee-Fung SD, Konofagou EE. ECG-gated, mechanical and electromechanical wave imaging of cardiovascular tissues in vivo. *Ultrasound Med. Biol.* 2007; 33:1075–1085. [PubMed: 17507146]
- Reddy AK, Taffet GE, Li YH, Lim SW, Pham TT, Pocius JS, Entman ML, Michael LH, Hartley CJ. Pulsed Doppler signal processing for use in mice: Applications. *IEEE Trans. Biomed. Eng.* 2005; 52:1771–1783. [PubMed: 16235663]
- Rivas F, Cobb FR, Bache RJ, Greenfield JC. Relationship between blood-flow to ischemic regions and extent of myocardial-infarction - Serial measurement of blood-flow to ischemic regions in dogs. *Circ.Res.* 1976; 38:439–447. [PubMed: 1269083]
- Sampath S, Kim JH, Lederman RJ, McVeigh ER. Simultaneous imaging of myocardial motion and chamber blood flow with SPAMM n' EGGs (spatial modulation of magnetization with encoded gradients for gauging speed). *J. Magn. Reson. Imaging.* 2008; 27:809–817. [PubMed: 18383258]
- Sengupta PP, Khandheria BK, Korinek J, Jahangir A, Yoshifuku S, Milosevic I, Belohlavek M. Left ventricular isovolumic flow sequence during sinus and paced rhythms - New insights from use of high-resolution Doppler and ultrasonic digital particle imaging velocimetry. *J. Am. Coll. Cardiol.* 2007; 49:899–908. [PubMed: 17320749]
- Shariati MA, Dripps JH, McDicken WN. A comparison of color-flow imaging algorithms. *Phys. Med. Biol.* 1993; 38:1589–1600. [PubMed: 8272434]
- Sugimoto N, Uyama C, Sugahara T, Yanagihara Y. Estimation of 2-d blood-flow velocity map from cine-angiograms - Algorithm using overlapping block set and illustration of vortex flow in abdominal aneurysm. *Med. Biol. Eng. Comput.* 1994; 32:S178–S184. [PubMed: 7967833]
- Sutherland GR, Di Salvo G, Claus P, D'hooge J, Bijnens B. Strain and strain rate imaging: A new clinical approach to quantifying regional myocardial function. *J. Am. Soc. Echocardiogr.* 2004; 17:788–802. [PubMed: 15220909]
- Tarnavski O, McMullen JR, Schinke M, Nie Q, Kong S, Izumo S. Mouse cardiac surgery: comprehensive techniques for the generation of mouse models of human diseases and their application for genomic studies. *Physiol. Genomics.* 2004; 16:349–360. [PubMed: 14679301]
- Taylor TW, Yamaguchi T. Three-dimensional simulation of blood-flow in an abdominal aortic-aneurysm - Steady and unsteady-flow cases. *J. Biomech. Eng.- Trans. ASME.* 1994; 116:89–97.
- Thibault H, Gomez L, Donal E, Augeul L, Scherrer-Crosbie M, Ovize M, Derumeaux G. Regional Myocardial Function After Myocardial Infarction in Mice: A Follow-Up Study by Strain Rate Imaging. *J. Am. Soc. Echocardiogr.* 2009; 22:198–205. [PubMed: 19121566]
- Thibault H, Gomez L, Donal E, Pontier G, Scherrer-Crosbie M, Ovize M, Derumeaux G. Acute myocardial infarction in mice: assessment of transmural by strain rate imaging. *Am. J. Physiol.-Heart Circul. Physiol.* 2007; 293:H496–H502.
- Tortoli P, Morganti T, Bambi G, Palombo C, Ramnarine KV. Noninvasive simultaneous assessment of wall shear rate and wall distension in carotid arteries. *Ultrasound Med. Biol.* 2006; 32:1661–1670. [PubMed: 17112953]
- Trahey GE, Allison JW, Vonramm OT. Angle independent ultrasonic-detection of blood-flow. *IEEE Trans. Biomed. Eng.* 1987; 34:965–967. [PubMed: 2961682]
- Vappou J, Zervantonakis IK, Luo J, Konofagou EE. Finite element modeling of the pulse wave propagation in the aorta for simulation of the pulse wave imaging (PWI) method. *MICCAI Workshop Proc.- Computational Biomechanics for Medicine III.* 2008:118–127.
- Walker WF, Trahey GE. A fundamental limit on the performance of correlation-based phase correction and flow estimation techniques. *IEEE Trans. Ultrason. Ferroelectr. Freq. Control.* 1994; 41:644–654.
- Wan Y, Liu D, Ebbini ES. Imaging vascular mechanics using ultrasound: Phantom and in vivo results. *Proc. of ISBI.* 2010:980–983.
- Wang S, Lee W-N, Provost J, Luo J, Konofagou EE. A composite high-frame-rate system for clinical cardiovascular imaging. *IEEE Trans. Ultrason. Ferroelectr. Freq. Control.* 2008; 55:2221–2233. [PubMed: 18986870]

- Watanabe H, Hisada T, Sugiura S, Okada J, Fukunari H. Computer simulation of blood flow, left ventricular wall motion and their interrelationship by fluid-structure interaction finite element method. *JSME Int. J. Ser. C-Mech. Syst. Mach. Elem. Manuf.* 2002; 45:1003–1012.
- Watanabe H, Sugano T, Sugiura S, Hisada T. Finite element analysis of ventricular wall motion and intra-ventricular blood flow in heart with myocardial infarction. *JSME Int. J. Ser. C-Mech. Syst. Mach. Elem. Manuf.* 2004; 47:1019–1026.
- Waterston RH, Lindblad-Toh K, Birney E, Rogers J, Abril JF, Agarwal P, Agarwala R, Ainscough R, Alexandersson M, An P, Antonarakis SE, Attwood J, Baertsch R, Bailey J, Barlow K, Beck S, Berry E, Birren B, Bloom T, Bork P, Botcherby M, Bray N, Brent MR, Brown DG, Brown SD, Bult C, Burton J, Butler J, Campbell RD, Carninci P, Cawley S, Chiaromonte F, Chinwalla AT, Church DM, Clamp M, Clee C, Collins FS, Cook LL, Copley RR, Coulson A, Couronne O, Cuff J, Curwen V, Cutts T, Daly M, David R, Davies J, Delehaunty KD, Deri J, Dermitzakis ET, Dewey C, Dickens NJ, Diekhans M, Dodge S, Dubchak I, Dunn DM, Eddy SR, Elnitski L, Emes RD, Eswara P, Eyras E, Felsenfeld A, Fewell GA, Flicek P, Foley K, Frankel WN, Fulton LA, Fulton RS, Furey TS, Gage D, Gibbs RA, Glusman G, Gnerre S, Goldman N, Goodstadt L, Grafham D, Graves TA, Green ED, Gregory S, Guigo R, Guyer M, Hardison RC, Haussler D, Hayashizaki Y, Hillier LW, Hinrichs A, Hlavina W, Holzer T, Hsu F, Hua A, Hubbard T, Hunt A, Jackson I, Jaffe DB, Johnson LS, Jones M, Jones TA, Joy A, Kamal M, Karlsson EK, Karolchik D, Kasprzyk A, Kawai J, Keibler E, Kells C, Kent WJ, Kirby A, Kolbe DL, Korfi I, Kucherlapati RS, Kulbokas EJ, Kulp D, Landers T, Leger JP, Leonard S, Letunic I, Levine R, Li J, Li M, Lloyd C, Lucas S, Ma B, Maglott DR, Mardis ER, Matthews L, Mauceli E, Mayer JH, McCarthy M, McCombie WR, McLaren S, McLay K, McPherson JD, Meldrum J, Meredith B, Mesirov JP, Miller W, Miner TL, Mongin E, Montgomery KT, Morgan M, Mott R, Mullikin JC, Muzny DM, Nash WE, Nelson JO, Nhan MN, Nicol R, Ning Z, Nusbaum C, O'Connor MJ, Okazaki Y, Oliver K, Larty EO, Pachter L, Parra G, Pepin KH, Peterson J, Pevzner P, Plumb R, Pohl CS, Poliakov A, Ponce TC, Ponting CP, Potter S, Quail M, Reymond A, Roe BA, Roskin KM, Rubin EM, Rust AG, Santos R, Sapojnikov V, Schultz B, Schultz J, Schwartz MS, Schwartz S, Scott C, Seaman S, Searle S, Sharpe T, Sheridan A, Shownkeen R, Sims S, Singer JB, Slater G, Smit A, Smith DR, Spencer B, Stabenau A, Strange-Thomann NS, Sugnet C, Suyama M, Tesler G, Thompson J, Torrents D, Trevaskis E, Tromp J, Ucla C, Vidal AU, Vinson JP, von Niederhausern AC, Wade CM, Wall M, Weber RJ, Weiss RB, Wendl MC, West AP, Wetterstrand K, Wheeler R, Whelan S, Wierzbowski J, Willey D, Williams S, Wilson RK, Winter E, Worley KC, Wyman D, Yang S, Yang SP, Zdobnov EM, Zody MC, Lander ES, Mouse Genome Sequencing C. Initial sequencing and comparative analysis of the mouse genome. *Nature.* 2002; 420:520–562. [PubMed: 12466850]
- Wehrens XHT, Kirchhoff S, Doevendans PA. Mouse electrocardiography: An interval of thirty years. *Cardiovasc. Res.* 2000; 45:231–237. [PubMed: 10728340]
- Williams R, Needles A, Cherin E, Zhou YQ, Henkelman RM, Adamson SL, Foster FS. Noninvasive ultrasonic measurement of regional and local pulse-wave velocity in mice. *Ultrasound Med. Biol.* 2007; 33:1368–1375. [PubMed: 17561330]
- Wise RG, Al-Shafei AIM, Carpenter TA, Hall LD, Huang CLH. Simultaneous measurement of blood and myocardial velocity in the rat heart by phase contrast MRI using sparse q-space sampling. *J. Magn. Reson. Imaging.* 2005; 22:614–627. [PubMed: 16193471]
- Yu SCM. Steady and pulsatile flow studies in abdominal aortic aneurysm models using particle image velocimetry. *Int. J. Heat Fluid Flow.* 2000; 21:74–83.
- Yu SCM, Zhao JB. A particle image velocimetry study on the pulsatile flow characteristics in straight tubes with an asymmetric bulge. *Proc. Inst. Mech. Eng. Part C-J. Eng. Mech. Eng. Sci.* 2000; 214:655–671.

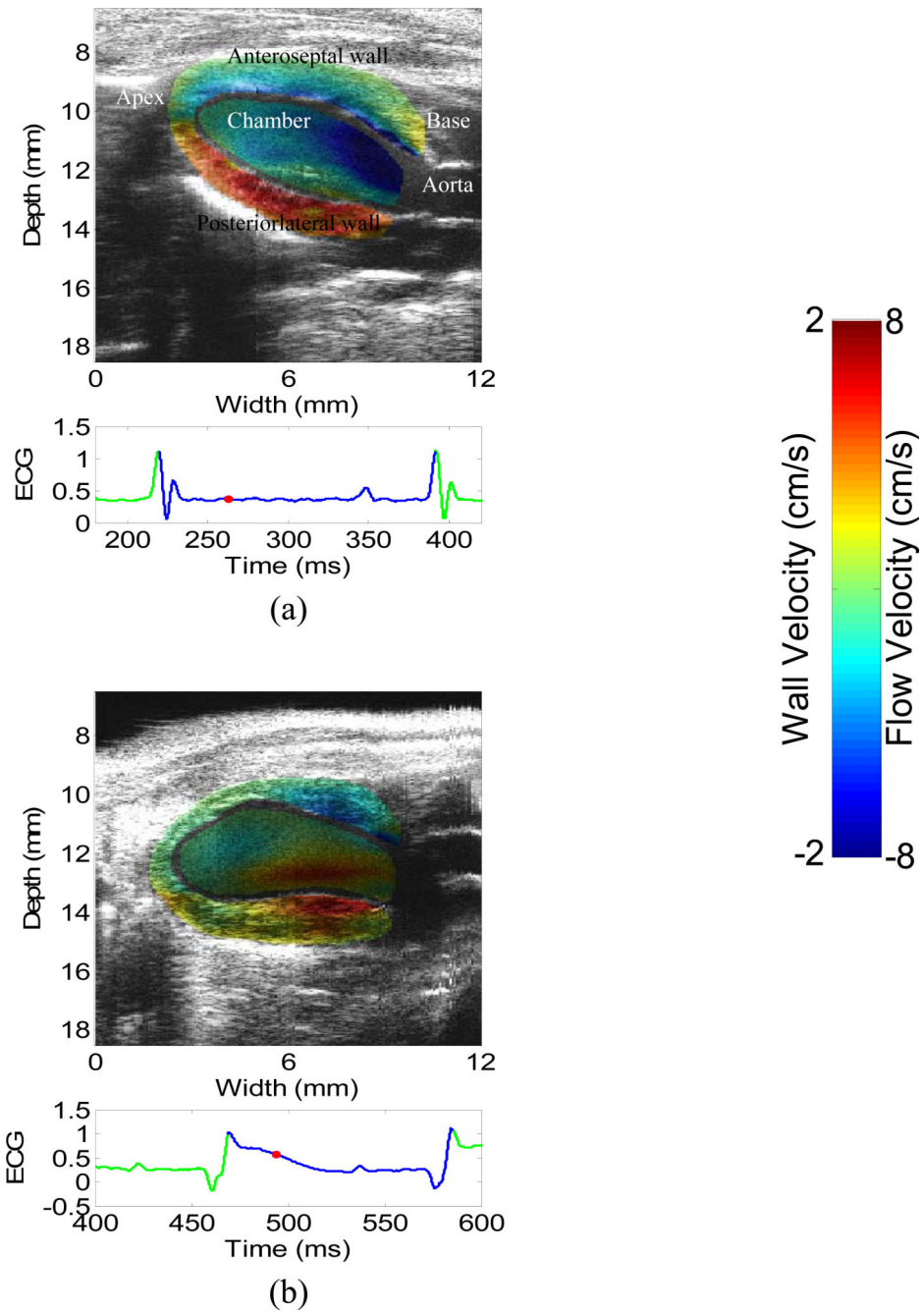


Figure 1.

2-D images of wall velocity and blood velocity in the systolic phase of (a) a normal and (b) an infarcted heart. The red dot on the ECG trace indicates the time in the cardiac cycle at which the image above it was acquired.

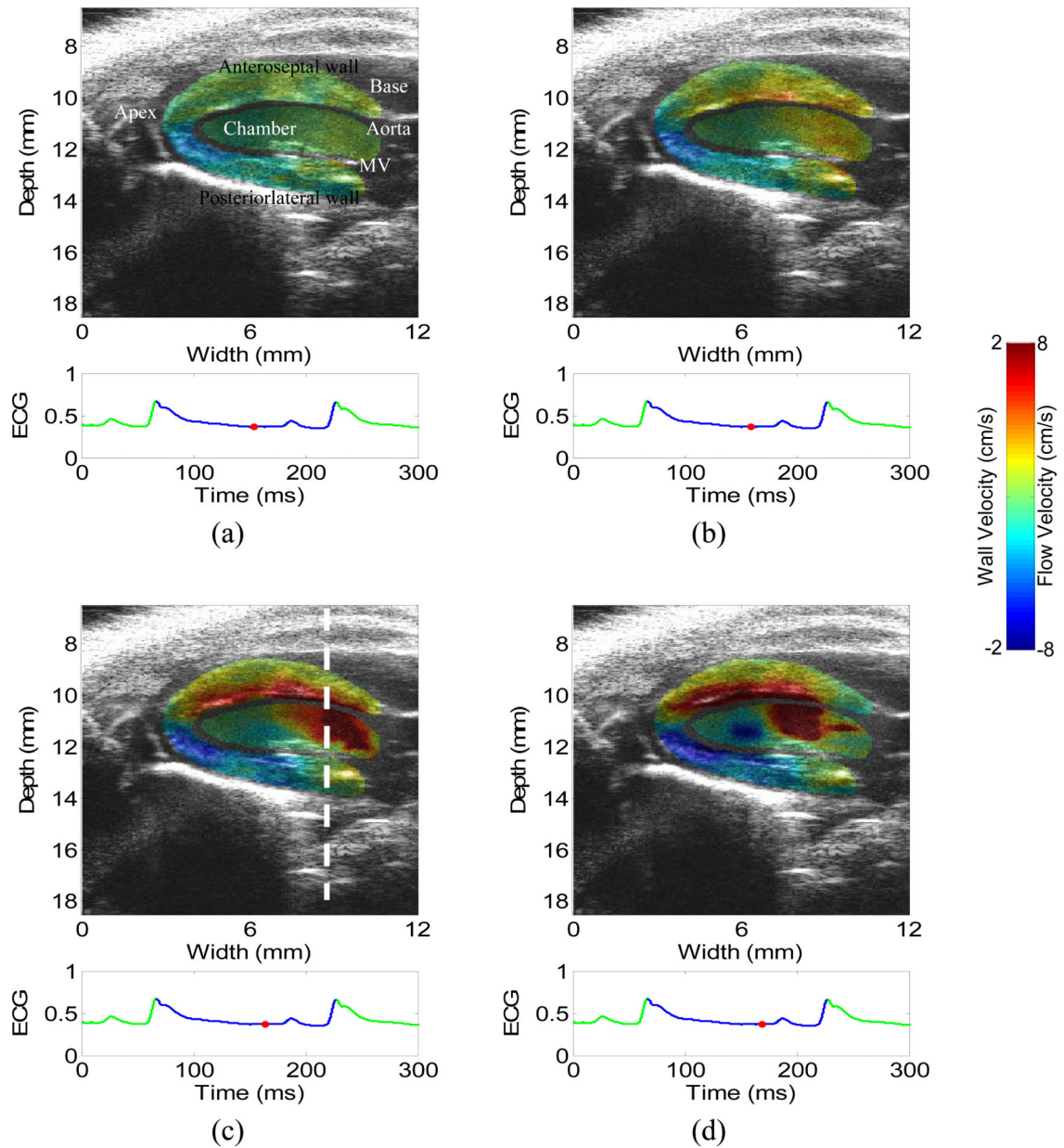


Figure 2.

2-D images of wall velocity and blood velocity in the diastolic phase of a normal heart, with 5 ms apart. (a) is before the mitral valve opens, i.e., isovolumic relaxation phase. (c-d) is immediately after the mitral valve opens, i.e., rapid filling phase. Opposite flows in (d) suggest the formation of a vortex, which is confirmed by the B-mode cine-loop. The mitral valve (MV) is visible in (a). The dashed line in (c) indicates the location of the M-mode image (Figs. 4(a) and 5(a)).

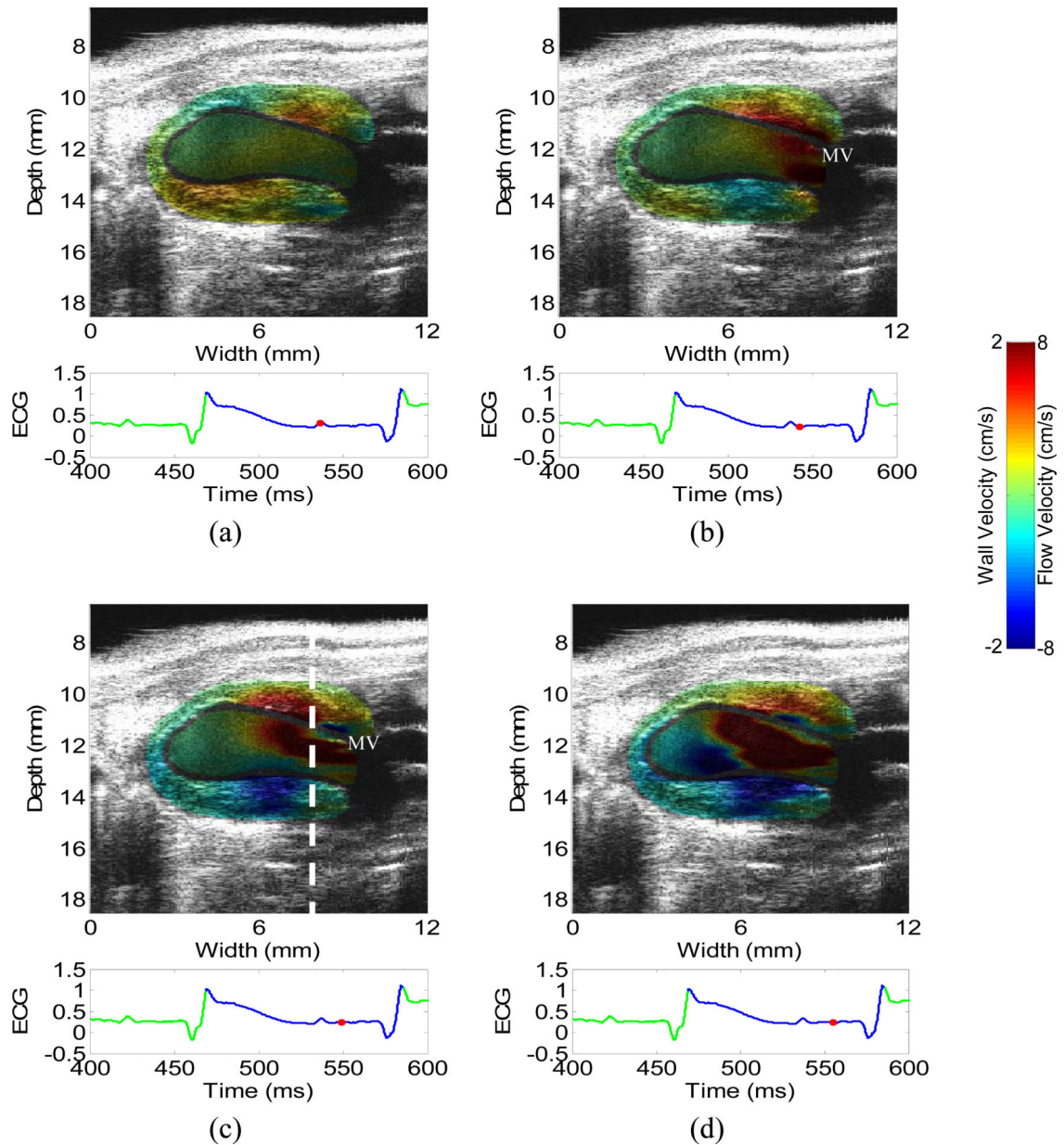


Figure 3.

2-D images of wall velocity and blood velocity in the diastolic phase of a normal heart, with 5 ms apart. (a) is before the mitral valve opens, i.e., isovolumic relaxation phase. (c-d) is immediately after the mitral valve opens, i.e., rapid filling phase. Opposite flows in (d) suggest the formation of a vortex, which was confirmed by the B-mode cine-loop. The dashed line in (c) indicates the location of the M-mode image (Figs. 4(b) and 5(b)). The mitral valve (MV) is visible in (b) and (c).

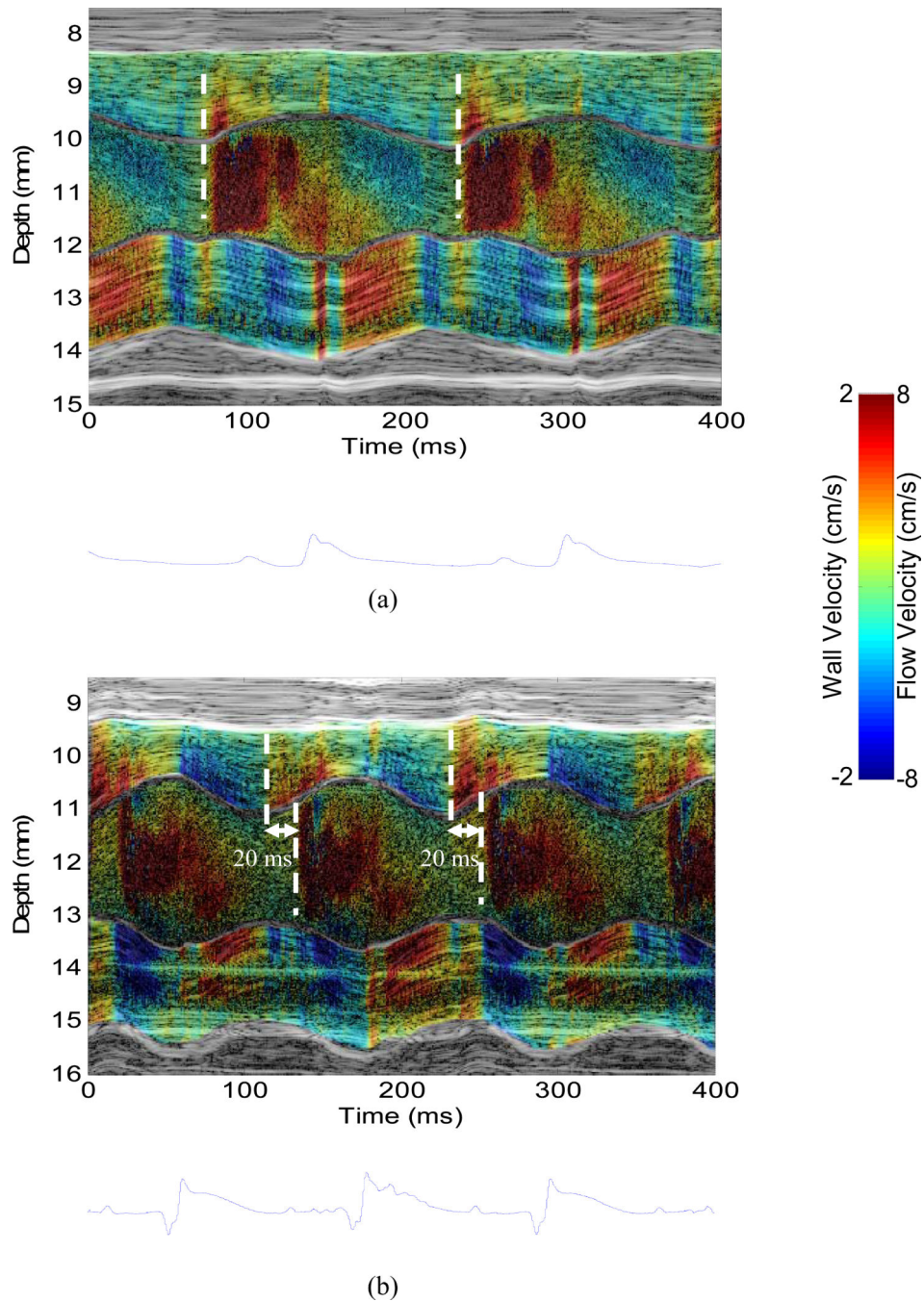


Figure 4.

M-mode image of (a) wall velocity and blood velocity in (a) the normal and (b) infarcted hearts, taken from the location indicated by the dashed line in Figs. 2(c) and 3(c), respectively. The dashed lines indicated the temporal onsets of wall velocity and blood velocity in diastole. The associated ECG trace was shown below the M-mode image.

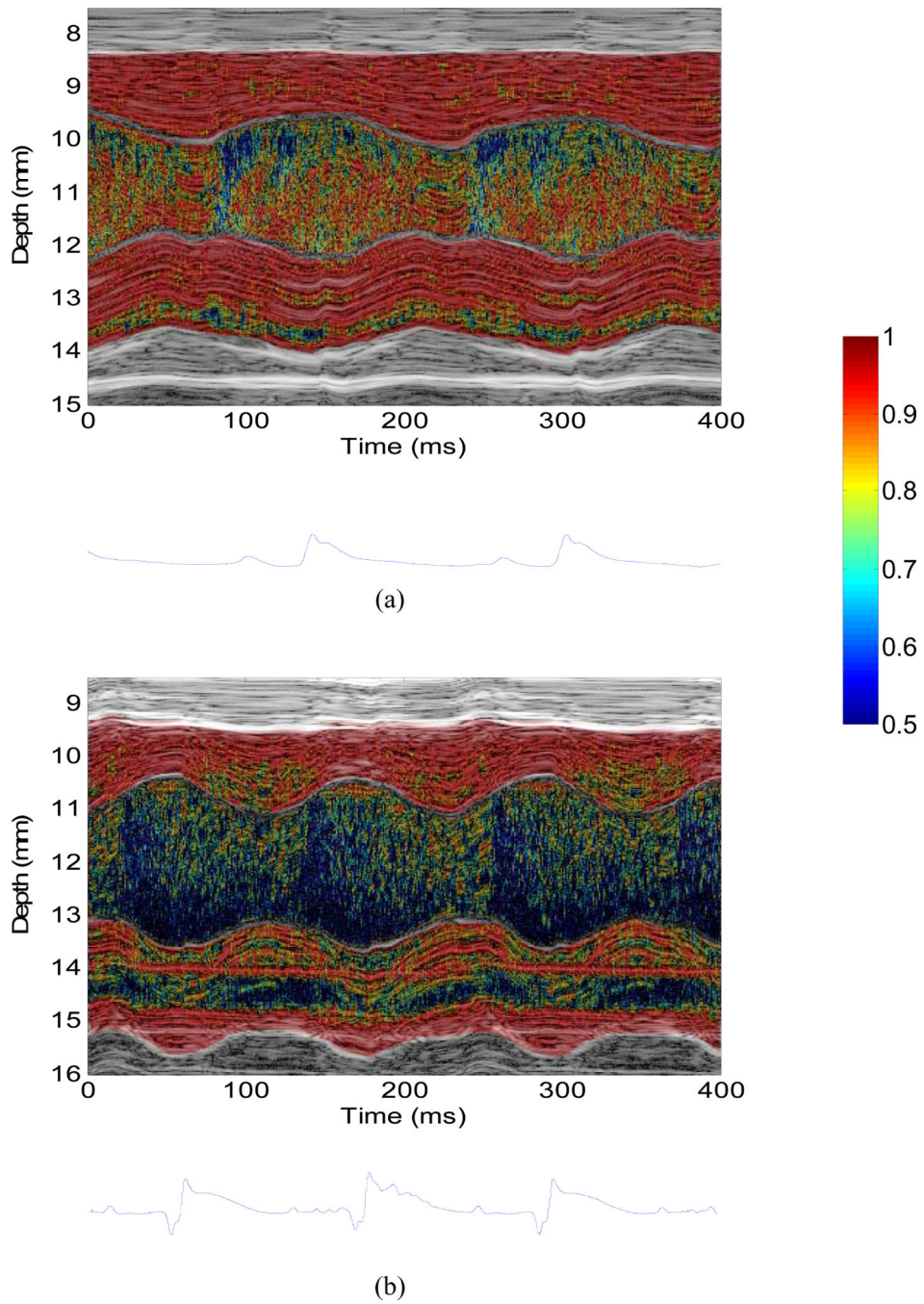


Figure 5.

M-mode image of the correlation coefficient in (a) the normal and (b) infarcted hearts, taken from the location indicated by the dashed line in Figs. 2 and 3, respectively. The associated ECG trace was shown below the M-mode image.

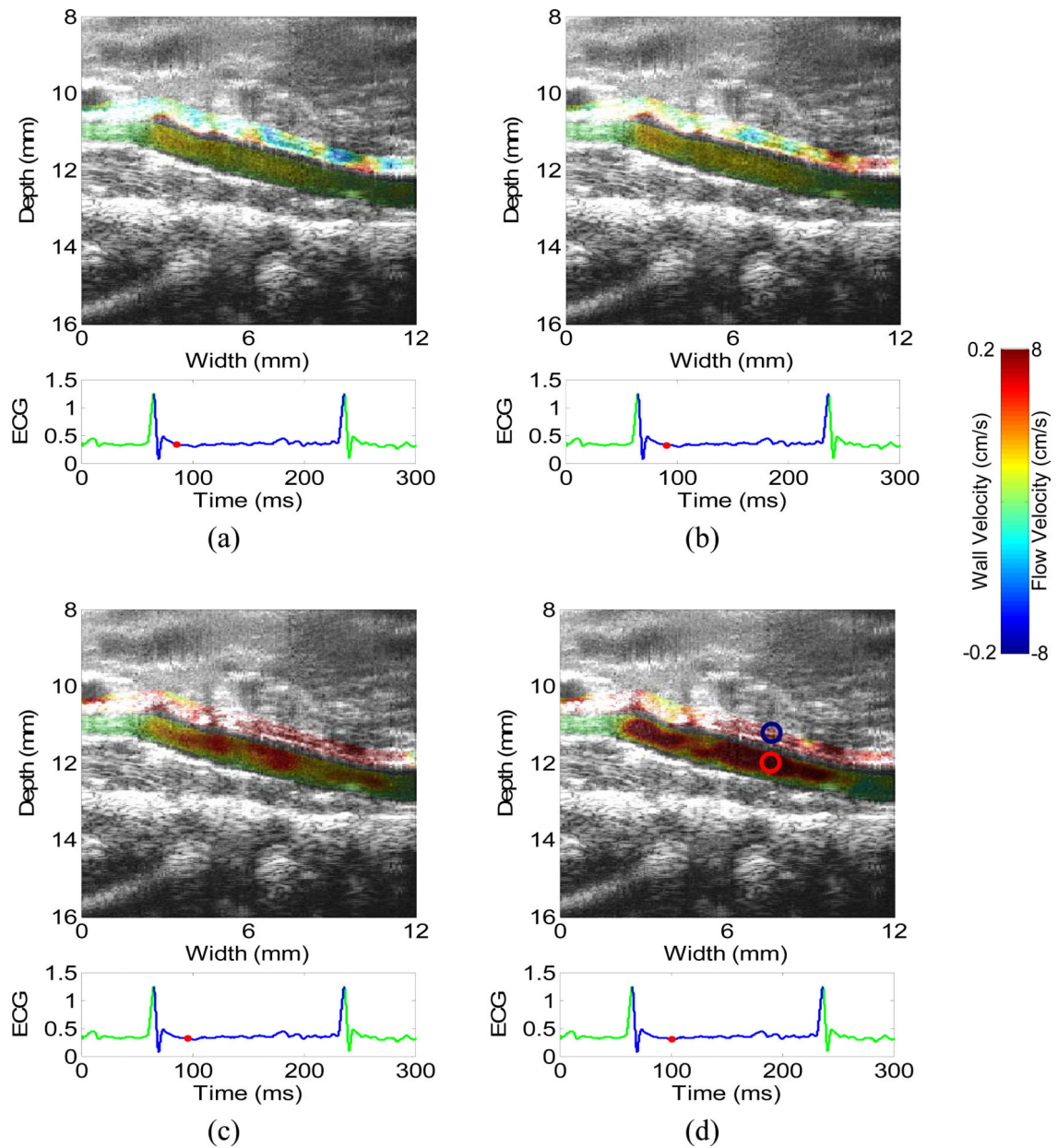


Figure 6.

2-D images of aortic wall velocity and lumen blood velocity in the systolic phase of a normal abdominal aorta (5 ms apart). The circles in (d) indicate where the waveforms in Fig. 7 are taken from. Only the velocities on the anterior aortic wall and the peri-aortic tissue as well as the lumen are shown.

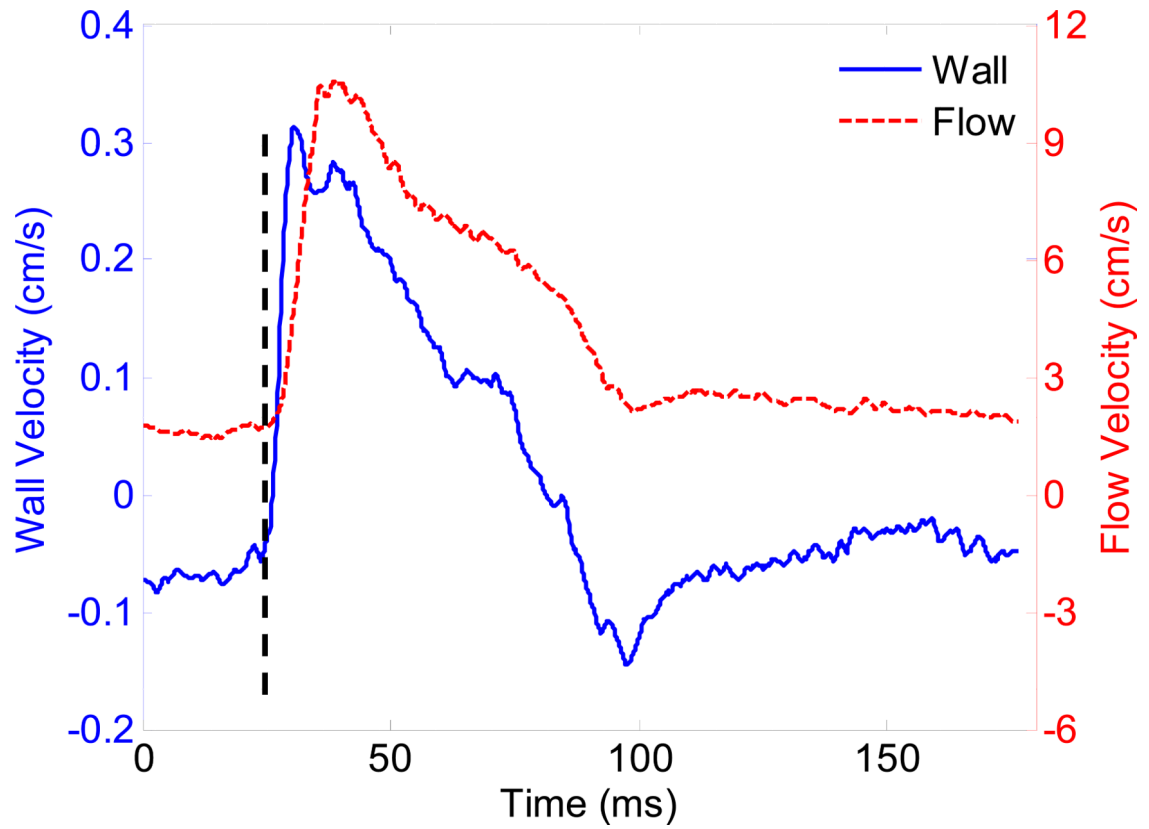


Figure 7.

Waveforms of wall velocity and blood velocity of the normal abdominal aorta in one cardiac cycle (from ECG R-wave peak to next R-wave peak), taken from the regions indicated by the circles in Fig. 6(d). The onsets of wall motion and blood velocity are synchronized, as indicated by the dashed line.

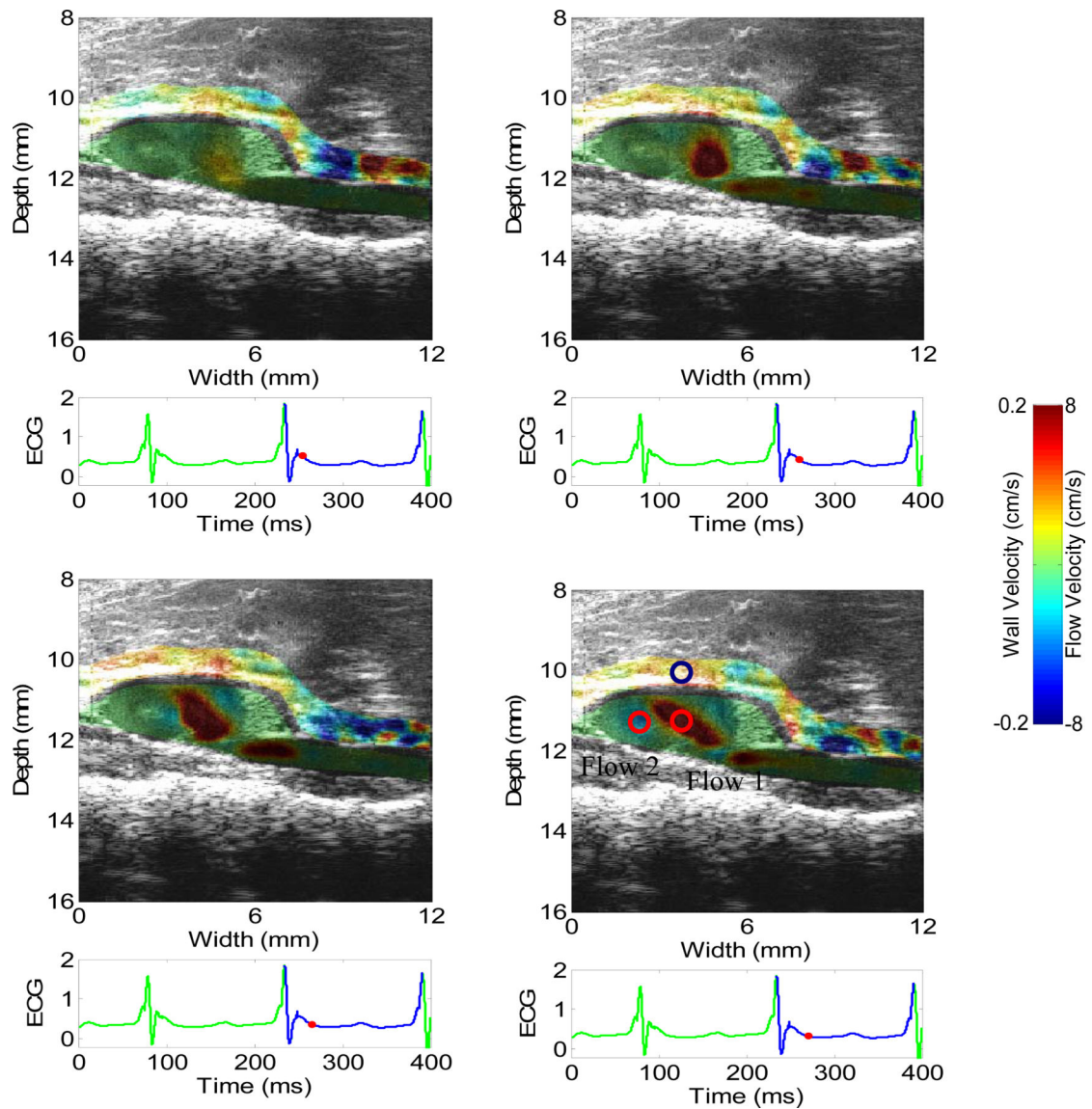


Figure 8.

2-D images of wall velocity and blood velocity in the systolic phase of an aneurysmal abdominal aorta (5 ms apart). The circles in (d) indicate where the waveforms in Fig. 9 are taken from. Only the velocities on the anterior aortic wall and the peri-aortic tissue as well as the lumen are shown.

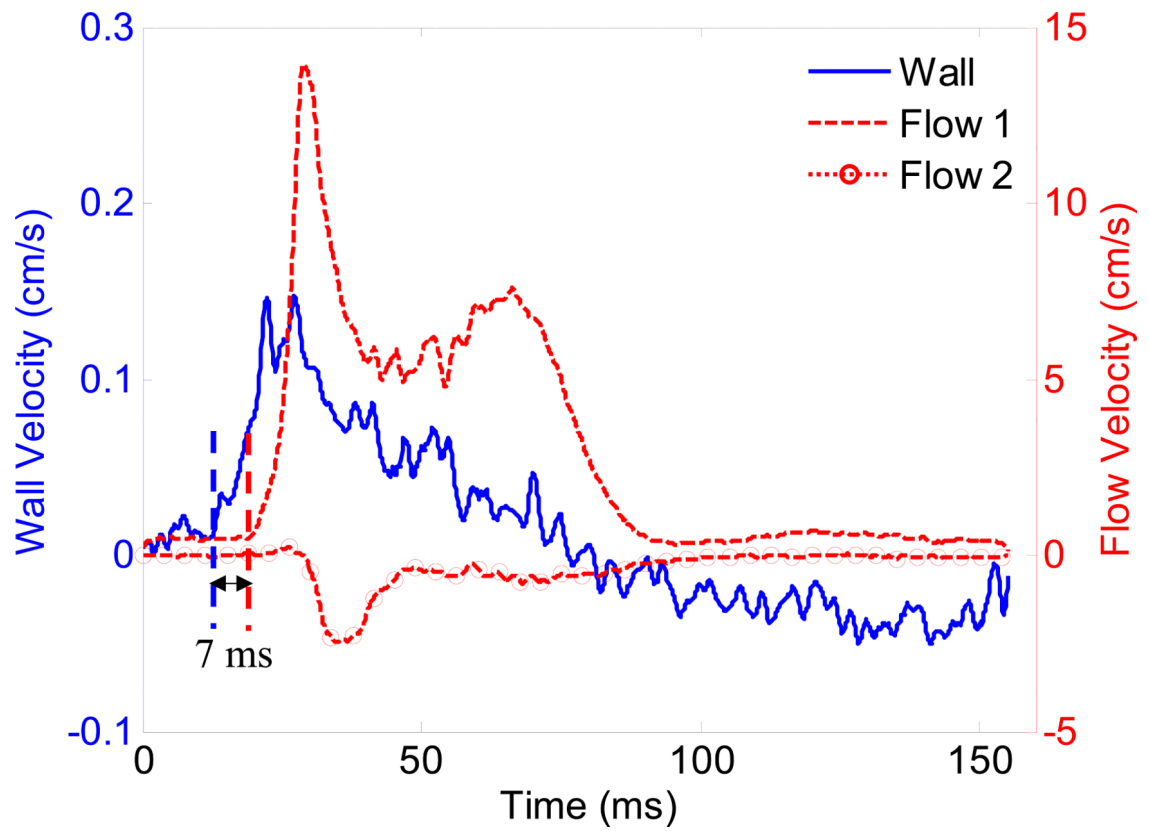


Figure 9.

Waveforms of wall motion and blood velocity of the aneurysmal abdominal aorta in one cardiac cycle (from ECG R-wave peak to next R-wave peak), taken from the regions indicated by the circles in Fig. 8(d). The onsets of wall motion and blood velocity are desynchronized.